

Controlling Ag diffusion in ZnO by donor doping: a first principles study

Tianwei Wang^a, Paul D. Bristowe^{a,*}

^a*Department of Materials Science and Metallurgy, University of Cambridge, Cambridge CB3 0FS, UK*

Abstract

Silver interdiffusion is often detrimental to the performance of thin-film coatings and devices that contain Ag/ZnO interfaces. Using a first principles computational analysis, a strategy is proposed which limits this diffusion by incorporating substitutional donor dopants into ZnO. First principles nudged elastic band calculations indicate that interstitial silver is likely to diffuse towards its nearby interstitial positions along [0001] in ZnO, with a relatively small energy barrier of 0.75 eV. Doping ZnO with Al slightly increases this energy barrier to 0.89 eV. In Sn-doped ZnO and Sc-doped ZnO, interstitial silver may bind to Sn or Sc and a neighbouring oxygen atom to form a Ag-O-Sn/Sc trimer in the ground state which increases the Ag migration barrier to 1.01 eV and 1.34 eV, respectively. An analysis of the Bader charges and bond strengths shows that electrostatic interactions and ionic radii have a more significant impact on Ag migration than charge transfer between the interstitial and its neighbours. In particular, the binding between Ag, O and Sn/Sc is found to be the main effect responsible for inhibiting Ag diffusion in doped ZnO.

Keywords: Ionic diffusion, Thin film coatings, Doped ZnO, First-principles calculation

1. Introduction

The excellent conductivity and transmittance of Ag/ZnO based thin-films has led to their wide use in a variety of industrial applications including low-emissivity multilayer coatings in the glass industry [1] and transparent electrodes for flat-panel displays, thin-film transistors
5 and solar cells [2, 3]. The deposition of silver on ZnO largely increases the conductivity of

*Corresponding author, tel: +44-(0)1223-334305.

Email addresses: tw445@cam.ac.uk (Tianwei Wang), pdb1000@cam.ac.uk (Paul D. Bristowe)

the thin-film system and simultaneously reduces its effective emissivity [4, 5]. In addition, doping the ZnO with, for example, small amounts of Al to form AZO (Al-doped ZnO) further enhances the transmittance and compensates for the reduced transparency as a result of the silver layer [1, 6]. The present generation of multilayer coatings requires them to be annealed
10 at a temperature up to 650 °C [7–9] in order to reduce defects, enhance the crystal structures, and optimise the optical and electrical properties [10–12].

Silver atoms are highly mobile at elevated temperatures and may diffuse into the nearby layers of a multilayer thin-film system [9]. Sahu *et al.* have carried out a series of experiments on the optical and electrical properties of Ag/AZO thin films. In one study [3] they reported
15 a Ag/AZO stack, deposited using electron beam evaporation, with an excellent resistivity of the order 10^{-5} $\Omega\cdot\text{cm}$ (2.5×10^{-4} $\Omega\cdot\text{cm}$ for AZO) and a transmittance of 85%. The Ag/AZO films produced could withstand a temperature of 500 °C, though in another study [13], they suspected that interdiffusion between the Ag and AZO layers was the cause of some measured changes in the photo-electric properties. A different AZO/Ag/AZO multilayer
20 stack deposited by radio frequency magnetron sputtering was studied by Crupi *et al.* [8], in which a similar resistivity of 1.8×10^{-5} $\Omega\cdot\text{cm}$ was measured. It was also noted in [8] that the AZO (compared to pure ZnO) film was a good barrier to Ag diffusion and contributed to the thermal stability of the multilayer up to 400 °C. Nevertheless, in both studies the thermal stability was investigated by comparing the optical and electrical properties of the thin-film
25 systems before and after annealing, while no direct data on silver diffusion (concentration profile, diffusivity, etc.) were provided. However, a detailed investigation of silver diffusion in AZO and Zn_2SnO_4 (ZTO) was conducted by Kulczyk-Malecka *et al.* [7], in which the films were heated to 250 °C and silver was found to diffuse rapidly into both materials within 5 min. Clearly this silver interdiffusion may have a detrimental effect on the functionality of
30 the coatings. However, the detailed diffusion mechanism in ZnO or AZO as well as across the Ag/ZnO interface remains unclear.

A first principles computational study by Huang *et al.* [14] has provided further insight

into this diffusion mechanism by simulating the migration of several potential acceptor dopants (Li, Na, K, and Ag) in ZnO. These elements were found to be fast diffusers
35 as interstitial dopants while substitutional dopants on the zinc site were relatively more stable. In addition, silver diffusion in ZnO was found to be anisotropic and vacancy-assisted. However, the effects of more than one dopant were not considered in this study.

In the present work, the atomistic mechanism for silver diffusion in donor doped ZnO is investigated in detail using a first principles computational technique based on density
40 functional theory (DFT). Three donor dopants (Al, Sc and Sn) are considered and compared with the goal of determining which would be best for controlling Ag diffusion in ZnO.

2. Computational Method

The first principles calculations were performed using the pseudopotential based plane-wave DFT code VASP [15, 16]. The generalised-gradient approximation (GGA) as parameterised
45 by Perdew, Burke and Ernzerhof (PBE) [17] was used for the exchange-correlation functional. The electronic wave functions were described using the projector augmented wave (PAW) method [18, 19]. A kinetic energy cutoff of 500 eV was chosen, providing a total energy convergence of less than 0.02 eV/atom. The self-consistency calculations were carried out with a Gaussian smearing width of 0.05 eV and a convergence tolerance of 1×10^{-9} eV.
50 Orthorhombic supercells were constructed from the primitive hexagonal cell of ZnO using the experimentally obtained lattice parameters ($a = b = 3.250 \text{ \AA}$ and $c = 5.207 \text{ \AA}$ [20]). The resulting supercell of pure ZnO contained 96 atoms (8 c -planes each with 12 atoms). Monkhorst-Pack k-point meshes of size $3 \times 3 \times 3$ were used for this supercell and a similar density of 0.03 \AA^{-1} was employed for other associated calculations (e.g. Al_2O_3 , Sc_2O_3 , and
55 SnO_2). The ionic geometry was optimised by the conjugate gradients (CG) algorithm with a convergence tolerance of 0.01 eV/\AA for the maximum force.

The migration barrier for silver diffusion in ZnO and doped ZnO was estimated using the climbing image nudged elastic band (CI-NEB) method [21, 22]. The CI-NEB code was

developed by Henkelman *et al.* [23] and implemented in VASP as VTST (Transition State
60 Tools for VASP). The NEB calculations used the same parameters and settings as were used
for the ground state calculations. The saddle points were relaxed using the quick-min (QM)
optimiser [24] with a convergence tolerance of 0.01 eV/Å. The ionic geometry was optimised
with the cell fixed in the NEB-related calculations, while the whole cell was relaxed when
calculating the defect formation energy.

65 Charge density analysis was performed using QTAIMAC (Quantum Theory of Atoms in
Molecules and Crystals) [25–27] as implemented in the Critic2 code [28, 29]. This analysis
provides information about the atomic charges (Bader charges) and the bond strengths
(charge densities at the bond critical points). Briefly, the QTAIMAC method divides a
70 crystal into disjoint regions called atomic basins by defining interatomic surfaces of electron
density which satisfy a zero-flux condition. Once the atomic basins are defined, atomic
properties such as Bader charges can be calculated by integrating the charge density inside
each atomic basin. The charge density topology is determined using critical points of charge
density where the gradient is zero. The first order saddle point of electron density is called
the bond critical point (bcp) and lies on a bond path that defines a bond between two atoms.
75 The charge density and its Laplacian at the bcp describe the strength and nature of the bond
respectively. The charge densities used for Critic2 were obtained from VASP using a denser
FFT (Fast Fourier Transform) grid.

The atomic structures were visualised using VESTA (Visualisation for Electronic and
Structural Analysis) software package by K. Momma *et al.* [30].

80 3. Results and Discussion

3.1. Formation of silver defects in ZnO

The supercells containing a single silver defect (substitutional or interstitial) were relaxed
and the energy of formation was computed using $\Delta E_f(d, q) = E_{tot}(d, q) - E_{tot}(h, q) + N_h\mu_h -$
 $N_d\mu_d + q\epsilon_F$, where $E_{tot}(d, q)$ is the total energy of the supercell with the defect and $E_{tot}(h, q)$

85 is the total energy of the perfect supercell containing only its original host atoms ($h = \text{Zn}$ or
 O for ZnO). N_h represents the number of substituted host atoms with chemical potential μ_h
 ($N_h = 0$ for interstitial dopants) and N_d is the number of defects with chemical potential μ_d .
 ϵ_F is the Fermi level. In this study the defect was assumed to be in a charge neutral state
 ($q = 0$). This assumption is based on the observation that nominally undoped ZnO is an
 90 n-type semiconductor probably due to the presence of native defects (e.g. oxygen vacancies)
 or interstitial hydrogen or both [31–34]. Previous DFT calculations [35] have shown that
 under n-type conditions, the silver interstitial, upon which this study will focus, prefers the
 charge neutral state. Furthermore, the three donor dopants introduced later also prefer the
 charge neutral state when substituted on a zinc site under the same conditions.

95 The oxygen-poor value of μ_{Zn} was computed from bulk Zn and the oxygen-rich value of μ_{O}
 was computed from a triplet oxygen molecule. In either environment, the chemical potentials
 satisfy the equilibrium condition $\mu_{\text{Zn}} + \mu_{\text{O}} = \mu_{\text{ZnO}}$. The chemical potential of Ag depends
 on the reservoir. Both bulk Ag and Ag_2O have been considered. However, it is known that
 the GGA functional overestimates the binding energy of an oxygen molecule [36, 37]. A
 100 correction to this binding energy has been obtained by comparing the calculated formation
 enthalpies of several transition metal oxides to experimental values (per O_2 molecule) and
 the difference was found to be 1.360 eV [37]. Thus, in the present study, the calculated O_2
 total energy (-9.857 eV) has been corrected to -8.497 eV and this agrees with the value used
 in a previous GGA-PAW study on defects in oxides [38].

Table 1: Formation energy (eV) of a Ag defect in bulk ZnO (reservoir: Ag)

	μ_{O}	μ_{Zn}	μ_{Ag}	$\Delta E_f(\text{Ag}_{\text{Zn}})$	$\Delta E_f(\text{Ag}_{\text{O}})$	$\Delta E_f(\text{Ag}_i)$
O-rich	-4.249	-4.681	-2.718	0.262	6.206	3.558
O-poor	-7.823	-1.106	-2.718	3.836	2.631	3.558

105 Tables 1 and 2 show that silver substitution on a zinc site is energetically preferred under
 oxygen-rich conditions while substitution on an oxygen site is the most favoured under

Table 2: Formation energy (eV) of a Ag defect in bulk ZnO (reservoir: Ag₂O)

	μ_{O}	μ_{Zn}	μ_{Ag}	$\Delta E_f(\text{Ag}_{\text{Zn}})$	$\Delta E_f(\text{Ag}_{\text{O}})$	$\Delta E_f(\text{Ag}_i)$
O-rich	-4.249	-4.681	-3.236	0.780	6.724	4.077
O-poor	-7.823	-1.106	-1.449	2.567	1.362	2.289

oxygen-poor conditions. This agrees with a recent database of computational results on doped ZnO provided by Yim *et al.* [35]. The interstitial silver defect always has the second lowest formation energy and these formation energies are relatively low. Thus, interstitial silver is also of great importance in ZnO [39, 40] and the main focus of the present work is on interstitial silver migration. Interestingly, interstitial silver occupies an asymmetric position in the hexagonal cage of ZnO unlike smaller ions such as Li, Na, and K [14]. There are three such positions in a single cage and this will influence the possible diffusion paths of Ag as illustrated in Fig. 1. The fractional coordinates of the positions are (0.3088, 0.1543, 0.6914), (0.8456, 0.1543, 0.6914), and (0.8456, 0.6912, 0.6914) as represented in the primitive cell of ZnO.

3.2. Silver migration in pure ZnO

The diffusion of silver interstitials in pure ZnO was studied using the NEB approach and the energy barriers of five different paths were estimated. The paths are illustrated in Fig. 1 and involve displacements along the a -, b -, and c -axes ($[2\bar{1}\bar{1}0]$, $[\bar{1}2\bar{1}0]$, and $[0001]$ directions).

The results are summarised in Table 3. The energy barriers along the a - and b - axes are less than 0.5 eV while the barriers along the c -axis are slightly larger but still less than 1.0 eV. Thus, diffusion along the c -axis is expected to be slower than along the a - or b -axis. The minimum energy paths (MEP) are shown in Fig. 2. The calculated barriers for paths (2), (4) and (5) agree well with the results by Huang *et al.* [14]. Due to the preferred $[0001]$ orientation of ZnO during epitaxial growth [41, 42], silver diffusion along the c -axis is of most interest. In fact the commonly observed orientation relation between ZnO and Ag is ZnO(0001)/Ag(111) [5]. During diffusion along the c -axis the silver interstitial passes

through one layer of zinc atoms and one layer of oxygen atoms, and thus paths (4) and
 130 (5) exhibit a double-barrier MEP, with the highest barrier occurring when the silver atom
 approaches the zinc layer.

Table 3: Calculated energy barrier for interstitial silver migration in pure ZnO.

	Orientation	Barrier (eV)
Path (1)	between nearby cages (b -axis)	0.12
Path (2)	in the same cage (a -axis)	0.45
Path (3)	through three cages (a - and b -axes)	0.49
Path (4)	c -axis	0.75
Path (5)	c -axis	0.89

3.3. Formation of Al, Sc and Sn defects in ZnO

It is well known that Al (few at.%) can be incorporated into ZnO as a donor dopant to
 improve its electrical and optical properties [43, 44]. However, the effects of subsequently
 135 introducing Ag into Al-doped ZnO are less well understood, particularly the chemical kinetics.
 Some studies have observed significant Ag diffusion in AZO [7], while others conclude that
 AZO can be a barrier to Ag diffusion [8]. Sc and Sn are also well known dopants in ZnO
 [45, 46], though Ag diffusion in these systems has not yet been investigated. In this work
 we compare the diffusion behaviour of Ag in AZO with that of diffusion in Sc and Sn-doped
 140 ZnO. First of all the formation energies of Al, Sc and Sn in ZnO were calculated using the
 computational method described in Section 3.1. The binary oxides of the dopants Al_2O_3 ,
 Sc_2O_3 , and SnO_2 were chosen as the reservoirs, as the chemical potentials μ_d ($d = \text{Al}, \text{Sc}, \text{Sn}$)
 were lower than in the bulk metal under both oxygen-rich and -poor conditions.

The energies of formation, both substitutional and interstitial, are shown in Table 4.
 145 It is seen that the preferred incorporation mechanism for each of these single dopants is
 substitution on the Zn site in both oxygen rich and poor conditions. This is significantly
 different from the Ag case where substitution on the O site was preferred in oxygen-poor

conditions. The predicted incorporation mechanism for Al, Sn, and Sc agrees well with previous studies, both computational [6, 35] and experimental [45–47]. It is seen that the formation energy of the Al_{Zn} defect under O-poor conditions is slightly negative. Other DFT calculations also obtain a value close to zero (e.g. ~ 0.2 eV [35]) suggesting that under these extreme conditions, which may be unlikely in practice, the defect would form freely.

In order to determine whether there is any tendency for the dopants to cluster in ZnO (which would affect Ag diffusion), the energy to form two or three dopants on neighbouring Zn sites was also studied. Six double substitutional and 12 triple substitutional configurations were considered. The dopant-dopant binding energy was obtained using $\Delta E_{\text{bind}}(n \cdot d_{\text{Zn}}) = \Delta E_f(n \cdot d_{\text{Zn}}) - n \cdot \Delta E_f(d_{\text{Zn}})$, where $\Delta E_f(n \cdot d_{\text{Zn}})$ is the total formation energy of n dopant atoms in ZnO and $\Delta E_f(d_{\text{Zn}})$ is the formation energy of a single dopant $d = \text{Al, Sc, or Sn}$ in ZnO. The binding energies were always found to be positive (0.2 eV to 0.6 eV) and thus these dopants do not readily cluster. Furthermore, in experiments, the dopant concentration is usually less than 2 at.% when doped ZnO thin-films are prepared [8, 45, 46]. In the calculations this corresponds to less than 2 dopant atoms in the 96-atom supercell. Consequently, in this study, silver migration along [0001] in ZnO is assumed to be affected by only one dopant atom.

Table 4: Calculated formation energies (eV) of single Al, Sc and Sn defects (d) in ZnO.

	μ_{O}	μ_{Zn}	μ_d	$\Delta E_f(d_{\text{Zn}})$	$\Delta E_f(d_{\text{O}})$	$\Delta E_f(d_i)$
Al (O-rich)	-4.249	-4.681	-12.330	1.690	16.557	10.088
Al (O-poor)	-7.823	-1.106	-6.968	-0.097	7.620	4.726
Sc (O-rich)	-4.249	-4.681	-16.203	2.210	15.378	9.706
Sc (O-poor)	-7.823	-1.106	-10.841	0.422	6.442	4.343
Sn (O-rich)	-4.249	-4.681	-10.275	3.917	14.311	10.715
Sn (O-poor)	-7.823	-1.106	-3.126	0.343	3.587	3.565

165 3.4. Silver migration in doped ZnO

The substitutional dopant was located along the migration path of the silver interstitial. Three possible initial positions for the Ag atom in the starting (0001) layer of the hexagonal cage and three possible final positions in the ending (0001) layer were considered (Fig. 3). The path along the c -axis was extended compared to that shown in Fig. 1 to allow
170 for full interaction with the dopant. The initial and final configurations for the NEB calculations were selected from the most energetically stable structures. The selected initial and final configurations of Ag in Al-doped ZnO had very similar total energies with a difference of less than 0.01 eV/atom. However, in the final configuration of the Sc- and Sn-doped structures, the Ag atom and the dopant were found to be bound with binding
175 energies of -0.033 and -0.084 eV, respectively. The binding energies were obtained using $\Delta E_{bind}(\text{Ag}_i, d_{\text{Zn}}) = \Delta E_f(\text{Ag}_i, d_{\text{Zn}}) - \Delta E_f(\text{Ag}_i) - \Delta E_f(d_{\text{Zn}})$ with $d = \text{Sc}$ or Sn . Thus, the initial and final configurations for Ag migration in Sc- or Sn-doped ZnO have different total energies, and the energy barrier for migration was computed relative to the low-energy structure containing the bound atoms.

180 The calculated migration paths are shown in Fig. 3. A similar extended migration path was also constructed for Ag in pure ZnO and the energy barrier was estimated to be 0.747 eV, which agreed well with the results of path (4) shown in Fig. 2. The calculated MEPs of these migration paths are given in Fig. 4. For pure ZnO, a 6-barrier MEP is seen since the silver atom passes through 3 layers of zinc atoms and 3 layers of oxygen atoms. Although the
185 complexity of the energy landscape increases when the ZnO is doped, multi-barrier MEPs were still observed. Slightly higher barriers of 0.89 and 1.01 eV were obtained for Ag in Al- and Sn-doped ZnO, respectively. The largest energy barrier of 1.34 eV was found in Sc-doped ZnO.

In order to understand better the physical origin of the different energy barriers, a charge
190 density analysis of each transition and ground (final) state has been performed using the QTAIMAC approach. With the help of these calculations, various possible explanations

including ionic size, electrostatic interactions, charge transfer effects and bond strengths have been considered. The effective ionic radii were approximated using the average distance between a particular nucleus and the relevant bond critical points. This was done in the neighbourhood of the Ag atom at the transition state (ts) or the ground state (gs). Table 5 compares these effective radii with standard database radii for ions in different coordinations [48]. It can be seen that Al has relatively the smallest radius which is consistent with the database. However, the relative ionic radii of Sc and Sn in either the transition or ground state configurations are reversed compared to the database values and Zn is predicted to be slightly smaller than Sc and Sn. Thus standard ionic radii do not necessarily reflect the effective radii of the ions during the migration of the Ag atom. This is highlighted by the result that the standard ionic radii increase in the order Al, Sn, Zn and Sc (6-fold coordination) while the Ag migration energy barrier increases for ZnO in the order undoped, Al-doped, Sn-doped and Sc-doped. Therefore, ionic size alone is not sufficient to explain the different energy barriers in doped ZnO. This is despite the fact that the effective ionic radius of Ag does not change much in either the transition or ground (final) state configurations.

The Bader charges on the atoms were also determined from the QTAIMAC calculations so as to investigate charge transfer and electrostatic effects during Ag migration (see Table 6). It is seen that the change in charge on both the Ag atom and the dopant atom at the ts configuration compared to the gs configuration increases in a very different order to the migration energy barrier. For example, the charge on the dopants increase in the order Al, Sc, Zn and Sn whereas the migration energy barrier increases in the order undoped, Al-doped, Sn-doped and Sc-doped. Furthermore, the magnitude of these charge differences is relatively small compared with the Bader charges themselves. Therefore, charge transfer between atoms during Ag migration may not be a significant factor that contributes to the energy barrier. However, the large Bader charge on Al has resulted in a large change in its electrostatic interaction (δE_{elec}) with the neighbouring Ag atom. Since Al exhibits an even smaller ionic radius than the Zn atom it replaces, it is reasonable to attribute the increase in

the energy barrier (relative to pure ZnO) to a large electrostatic effect in the case of AZO.

Table 5: Standard ionic radii (\AA) for Zn, Al, Sc and Sn in different coordinations (iv-vi) [48]. The effective ionic radii (r_{ts} and r_{gs}) were approximated using the average distance between the nucleus and bond critical points obtained from the QTAIMAC calculations. r_{ts} and r_{gs} refer to the radii in the transition and ground (final) states.

	r_{iv}	r_v	r_{vi}		$r_{ts}(d_{Zn})$	$r_{gs}(d_{Zn})$	$r_{ts}(Ag_i)$	$r_{gs}(Ag_i)$
Zn	0.60	0.68	0.74	$d = \text{Zn}$	0.953	0.951	1.287	1.324
Al	0.39	0.48	0.54	$d = \text{Al}$	0.760	0.789	1.303	1.338
Sc	n.a	n.a.	0.75	$d = \text{Sc}$	1.067	0.984	1.327	1.343
Sn	0.55	0.62	0.69	$d = \text{Sn}$	1.254	1.151	1.280	1.320

Table 6: Bader charges b (e) on the atoms of interest and their electrostatic interaction with the neighbouring Ag atom. The electrostatic interaction ($e^2/\text{\AA}$) was approximated using $E_{elec} = \frac{b_1 b_2}{l_{12}}$, where b is the Bader charge and l is the interatomic distance in \AA . δb and δE_{elec} are the differences between the transition and ground (final) states. Zn represents the Zn atom on its lattice site in pure ZnO.

	$b_{ts}(d_{Zn})$	$b_{ts}(Ag_i)$	l_{ts}	E_{elec}^{ts}	$b_{gs}(d_{Zn})$	$b_{gs}(Ag_i)$	l_{gs}	E_{elec}^{gs}	$\delta b(d_{Zn})$	$\delta b(Ag_i)$	δE_{elec}
Zn	1.162	0.429	2.381	0.209	1.251	0.400	4.227	0.118	-0.089	0.029	0.091
Al	2.430	0.333	2.496	0.322	2.451	0.311	4.082	0.186	-0.021	0.022	0.136
Sc	1.676	0.371	2.563	0.243	1.747	0.334	4.174	0.140	-0.071	0.037	0.103
Sn	1.386	0.408	2.579	0.219	1.512	0.379	4.206	0.136	-0.126	0.029	0.083

220

The electrostatic effect also supports the energy barrier difference between Sc and Sn, but it is still insufficient to explain their large barriers compared with Ag migration in pure ZnO ($\delta E_{elec}^{Sc} > \delta E_{elec}^{Zn} > \delta E_{elec}^{Sn}$). As mentioned earlier in this section, Sc and Sn were found to bind with the Ag interstitial and a neighbouring oxygen atom. Similar configurations were found during Ag migration in pure ZnO and AZO, though the binding energies were not negative.

225

The bound trimers are shown in Fig. 5 and the strengths of the bonds in the trimers are

given in Table 7. It is seen that the average bond strengths in the bound trimers are larger than in the non-bound cases (ZnO and AZO). Thus, the Ag-O-Sc/Sn bound trimers with large bond strengths produce a more energetically stable ground (final) state configuration and it is this that has the largest effect on the energy barrier.

Table 7: Bond strengths (f) and bond lengths (l) in the Ag-O- d trimers ($d = \text{Zn, Al, Sc, Sn}$). Bond strengths are in $1/\text{bohr}^3$ and bond lengths are in \AA . f_{ave} is the average strength.

	$f_{\text{Ag-O}}$	$l_{\text{Ag-O}}$	$f_{d_{\text{Zn-O}}}$	$l_{d_{\text{Zn-O}}}$	f_{ave}
Pure ZnO	0.082	2.412	0.052	2.210	0.067
Al-doped ZnO	0.067	2.228	0.060	1.959	0.066
Sc-doped ZnO	0.073	2.193	0.075	2.109	0.076
Sn-doped ZnO	0.075	2.182	0.076	2.195	0.076

230

In summary, silver diffusion in ZnO is a complex process involving the relative ionic sizes, electrostatics and the binding of silver with the dopant, all of which contribute to a lesser or greater extent to the energy barrier for migration. The different influence of each of these factors is shown schematically in Table 8.

Table 8: Schematic representation of the various factors contributing to the Ag migration barrier in doped ZnO. The total effect represents an increase in energy barrier relative to pure ZnO.

	Ionic Size Effect	Electrostatics	Binding Effect	Total Effect	Barrier (eV)
Pure ZnO					0.75
Al-doped ZnO	--	+++		+	0.89
Sc-doped ZnO	+	+	++	++++	1.34
Sn-doped ZnO	+	-	++	++	1.01

4. Conclusions

235 Interstitial silver migration in pure and doped ZnO has been studied using first principles calculations based on density functional theory. The migration barrier for silver diffusion in the basal plane of pure ZnO varies between 0.12 and 0.49 eV, while the barrier along [0001] is 0.75 eV. To limit interdiffusion at Ag(111)/ZnO(0001) interfaces, the migration barrier along [0001] should be increased. This study has shown that substitutional doping of ZnO
240 with donor dopants can accomplish this. In particular, incorporating Al, Sn, or Sc increases the migration barrier to 0.89, 1.01 and 1.34 eV, respectively. Thus, doping ZnO with a few at.% Sc, for example, is expected to be an effective solution to the problem of silver diffusion observed during the annealing of optical coatings. The calculations show that electrostatic interactions and ionic radii have a more significant impact on Ag migration than charge
245 transfer between the interstitial and its neighbours. In particular, the binding between Ag, O and Sn/Sc is found to be the main effect responsible for inhibiting Ag diffusion in doped ZnO.

Acknowledgements

T. Wang would like to thank the Cambridge Trust and the China Scholarship Council for
250 financial support. The calculations were performed at the Cambridge HPCS and the UK National Supercomputing Service, ARCHER. Access to the latter was obtained via the UKCP consortium and Materials Chemistry consortium which are both funded by EPSRC under Grant Nos. EP/K014560/1 and EP/L000202 respectively. Useful discussions with Dr. Paul Warren are gratefully acknowledged. All the necessary computational data are included
255 in the manuscript or the University of Cambridge Data Repository, <https://doi.org/10.17863/CAM.11020>.

References

- [1] J. A. Ridealgh, Large Area Coatings for Architectural Glass Design, Manufacturing, Process Faults, MRS Proceedings 890 (2005) 0890–Y01–10. doi:10.1557/PROC-0890-Y01-10.

- 260 [2] G. Teucher, T. Van Gestel, M. Krott, H. G. Gehrke, R. A. Eichel, S. Uhlenbruck, Processing of Al-doped ZnO protective thin films on aluminum current collectors for lithium ion batteries, *Thin Solid Films* 619 (2016) 302–307. doi:10.1016/j.tsf.2016.10.047.
- [3] D. R. Sahu, J. L. Huang, Development of ZnO-based transparent conductive coatings, *Solar Energy Materials and Solar Cells* 93 (11) (2009) 1923–1927. doi:10.1016/j.solmat.2009.07.004.
- 265 [4] G. Wang, L. Zhao, H. Diao, W. Wang, Optical enhancement by back reflector with ZnO:Al₂O₃(AZO) or NiCr diffusion barrier for amorphous silicon germanium thin film solar cells, *Vacuum* 89 (2013) 40–42. doi:10.1016/j.vacuum.2012.08.014.
- 270 [5] Z. Lin, P. D. Bristowe, Microscopic characteristics of the Ag (111) ZnO (0001) interface present in optical coatings, *Physical Review B - Condensed Matter and Materials Physics* 75 (20) (2007) 205423. doi:10.1103/PhysRevB.75.205423.
- [6] Z. Lin, P. D. Bristowe, A first principles study of the properties of Al:ZnO and its adhesion to Ag in an optical coating, *Journal of Applied Physics* 106 (1) (2009) 013520. doi:10.1063/1.3159651.
- 275 [7] J. Kulczyk-Malecka, P. J. Kelly, G. West, G. C. B. Clarke, J. A. Ridealgh, Investigations of diffusion behaviour in Al-doped zinc oxide and zinc stannate coatings, *Thin Solid Films* 520 (5) (2011) 1368–1374. doi:10.1016/j.tsf.2011.08.076.
- [8] I. Crupi, S. Boscarino, V. Strano, S. Mirabella, F. Simone, A. Terrasi, Optimization of ZnO:Al/Ag/ZnO:Al structures for ultra-thin high-performance transparent conductive electrodes, *Thin Solid Films* 520 (13) (2012) 4432–4435. doi:10.1016/j.tsf.2012.02.080.
- 280 [9] J. Kulczyk-Malecka, P. J. Kelly, G. West, G. C. B. Clarke, J. A. Ridealgh, K. P. Almqvist, A. L. Greer, Z. H. Barber, Investigation of silver diffusion in TiO₂/Ag/TiO₂ coatings, *Acta Materialia* 66 (2014) 396–404. doi:10.1016/j.actamat.2013.11.030.
- 285 [10] G. J. Fang, D. Li, B. L. Yao, Influence of post-deposition annealing on the properties of transparent conductive nanocrystalline ZAO thin films prepared by RF magnetron sputtering with highly conductive ceramic target, *Thin Solid Films* 418 (2) (2002) 156–162. doi:10.1016/S0040-6090(02)00733-2.

- 290 [11] S.-s. Lin, J.-l. Huang, P. Šajgalik, The properties of heavily Al-doped ZnO films before
and after annealing in the different atmosphere, *Surface and Coatings Technology* 185
(2004) 254–263. doi:10.1016/j.surfcoat.2003.12.007.
- [12] P. Nunes, D. Costa, E. Fortunato, R. Martins, Performances presented by zinc oxide
thin films deposited by r.f. magnetron sputtering, *Vacuum* 64 (3-4) (2002) 293–297.
295 doi:10.1016/S0042-207X(01)00323-2.
- [13] D. Sahu, S.-Y. Lin, J.-L. Huang, Study on the electrical and optical properties of
Ag/Al-doped ZnO coatings deposited by electron beam evaporation, *Applied Surface
Science* 253 (11) (2007) 4886–4890. doi:10.1016/j.apsusc.2006.10.061.
- [14] G.-Y. Huang, C.-Y. Wang, J.-T. Wang, First-principles study of diffusion of Li, Na, K
and Ag in ZnO, *Journal of Physics: Condensed Matter* 21 (34) (2009) 345802. doi:
300 10.1088/0953-8984/21/34/345802.
- [15] G. Kresse, J. Hafner, Ab initio molecular dynamics for liquid metals, *Physical Review B*
47 (1) (1993) 558–561. arXiv:0927-0256(96)00008, doi:10.1103/PhysRevB.47.558.
- [16] G. Kresse, J. Furthmüller, Efficient iterative schemes for ab initio total-energy
305 calculations using a plane-wave basis set, *Physical Review B* 54 (16) (1996) 11169–11186.
arXiv:0927-0256(96)00008, doi:10.1103/PhysRevB.54.11169.
- [17] J. P. Perdew, K. Burke, M. Ernzerhof, Generalized Gradient Approximation Made
Simple, *Physical Review Letters* 77 (18) (1996) 3865–3868. arXiv:0927-0256(96)
00008, doi:10.1103/PhysRevLett.77.3865.
- 310 [18] J. Lehtomäki, I. Makkonen, M. A. Caro, A. Harju, O. Lopez-Acevedo, Orbital-Free
Density Functional Theory Implementation with the Projector Augmented-Wave
Method, *Physical Review B* 50 (24) (2014) 17953–17979. arXiv:1408.4701, doi:
10.1063/1.4903450.
- [19] G. Kresse, From ultrasoft pseudopotentials to the projector augmented-wave method,
315 *Physical Review B* 59 (3) (1999) 1758–1775. doi:10.1103/PhysRevB.59.1758.
- [20] S. C. Abrahams, J. L. Bernstein, Remeasurement of the structure of hexagonal ZnO,
Acta Crystallographica Section B Structural Crystallography and Crystal Chemistry
25 (7) (1969) 1233–1236. doi:10.1107/S0567740869003876.
- [21] G. Henkelman, B. P. Uberuaga, H. Jónsson, Climbing image nudged elastic band method
320 for finding saddle points and minimum energy paths, *Journal of Chemical Physics*
113 (22) (2000) 9901–9904. doi:10.1063/1.1329672.

- [22] H. Jónsson, G. Mills, K. W. Jacobsen, Nudged elastic band method for finding minimum energy paths of transitions, in: *Classical and Quantum Dynamics in Condensed Phase Simulations*, WORLD SCIENTIFIC, 1998, pp. 385–404. doi: 10.1142/9789812839664_0016.
- [23] G. Henkelman, H. Jónsson, Improved tangent estimate in the nudged elastic band method for finding minimum energy paths and saddle points, *Journal of Chemical Physics* 113 (22) (2000) 9978–9985. doi:10.1063/1.1323224.
- [24] D. Sheppard, R. Terrell, G. Henkelman, Optimization methods for finding minimum energy paths, *Journal of Chemical Physics* 128 (13) (2008) 1–10. doi:10.1063/1.2841941.
- [25] R. F. W. Bader, *Atoms in Molecules. A Quantum Theory*, Oxford University Press, Oxford, 1990.
- [26] R. F. W. Bader, A quantum theory of molecular structure and its applications, *Chemical Reviews* 91 (5) (1991) 893–928. doi:10.1021/cr00005a013.
- [27] C. F. Matta, R. J. Boyd, *An Introduction to the Quantum Theory of Atoms in Molecules*, Wiley-VCH Verlag GmbH & Co. KGaA, Weinheim, Germany, 2007. doi: 10.1002/9783527610709.ch1.
- [28] A. Otero-de-la Roza, V. Luaña, A fast and accurate algorithm for QTAIM integration in solids, *Journal of Computational Chemistry* 32 (2) (2011) 291–305. arXiv: NIHMS150003, doi:10.1002/jcc.21620.
- [29] A. Otero-de-la Roza, E. R. Johnson, V. Luaña, Critic2: A program for real-space analysis of quantum chemical interactions in solids, *Computer Physics Communications* 185 (3) (2014) 1007–1018. doi:10.1016/j.cpc.2013.10.026.
- [30] K. Momma, F. Izumi, VESTA 3 for three-dimensional visualization of crystal, volumetric and morphology data, *Journal of Applied Crystallography* 44 (6) (2011) 1272–1276. doi:10.1107/S0021889811038970.
- [31] L. Liu, Z. Mei, A. Tang, A. Azarov, A. Kuznetsov, Q. K. Xue, X. Du, Oxygen vacancies: The origin of n-type conductivity in ZnO, *Physical Review B - Condensed Matter and Materials Physics* 93 (23) (2016) 1–6. doi:10.1103/PhysRevB.93.235305.
- [32] A. Janotti, J. B. Varley, J. L. Lyons, C. G. Van de Walle, Controlling the Conductivity in Oxide Semiconductors, in: J. Wu, J. Cao, W.-Q. Han, A. Janotti, H.-C. Kim (Eds.),

Functional Metal Oxide Nanostructures. Springer Series in Materials Science, Vol. 149, Springer, New York, NY, 2012, pp. 23–35. doi:10.1007/978-1-4419-9931-3_2.

- 355 [33] A. Janotti, C. G. Van de Walle, Fundamentals of zinc oxide as a semiconductor, Rep Prog Phy 72 (12) (2009) 126501. doi:10.1088/0034-4885/72/12/126501.
- [34] F. Oba, M. Choi, A. Togo, I. Tanaka, Point defects in ZnO: an approach from first principles, Science and Technology of Advanced Materials 12 (3) (2011) 034302. doi:10.1088/1468-6996/12/3/034302.
- 360 [35] K. Yim, J. Lee, D. Lee, M. Lee, E. Cho, H. S. Lee, H.-H. Nahm, S. Han, Property database for single-element doping in ZnO obtained by automated first-principles calculations, Scientific Reports 7 (December 2016) (2017) 40907. doi:10.1038/srep40907.
- [36] Y. L. Lee, J. Kleis, J. Rossmeisl, D. Morgan, Ab initio energetics of LaBO₃ (001) (B=Mn, Fe, Co, and Ni) for solid oxide fuel cell cathodes, Physical Review B - Condensed Matter and Materials Physics 80 (22) (2009) 1–20. doi:10.1103/PhysRevB.80.224101.
- 365 [37] L. Wang, T. Maxisch, G. Ceder, Oxidation energies of transition metal oxides within the GGA+U framework, Physical Review B - Condensed Matter and Materials Physics 73 (19) (2006) 195107. arXiv:9605103, doi:10.1103/PhysRevB.73.195107.
- 370 [38] C. Zhang, P. D. Bristowe, First principles calculations of oxygen vacancy formation in barium-strontium-cobalt-ferrite, RSC Advances 3 (30) (2013) 12267. doi:10.1039/c3ra41585f.
- [39] Q. Wan, Z. Xiong, J. Dai, J. Rao, F. Jiang, First-principles study of Ag-based p-type doping difficulty in ZnO, Optical Materials 30 (6) (2008) 817–821. doi:10.1016/j.optmat.2007.02.051.
- 375 [40] F. Yaqoob, M. Huang, Effects of high-dose hydrogen implantation on defect formation and dopant diffusion in silver implanted ZnO crystals, Journal of Applied Physics 120 (4) (2016) 045101. doi:10.1063/1.4958849.
- 380 [41] M. Arbab, Base layer effect on the d.c. conductivity and structure of direct current magnetron sputtered thin films of silver, Thin Solid Films 381 (1) (2001) 15–21. doi:10.1016/S0040-6090(00)01341-9.

- [42] N. Jedrecy, G. Renaud, R. Lazzari, J. Jupille, Flat-top silver nanocrystals on the two polar faces of ZnO: An all angle x-ray scattering investigation, Physical Review B - Condensed Matter and Materials Physics 72 (4) (2005) 045430. doi:10.1103/PhysRevB.72.045430.
- [43] A. Nakrela, N. Benramdane, A. Bouzidi, Z. Kebbab, M. Medles, C. Mathieu, Site location of Al-dopant in ZnO lattice by exploiting the structural and optical characterisation of ZnO: Al thin films, Results in Physics 6 (2016) 133–138. doi:10.1016/j.rinp.2016.01.010.
- [44] T. Coman, D. Timpu, V. Nica, C. Vitelaru, A. P. Rambu, G. Stoian, M. Olaru, C. Ursu, Sequential PLD in oxygen/argon gas mixture of Al-doped ZnO thin films with improved electrical and optical properties, Applied Surface Science 418 (2017) 456–462. doi:10.1016/j.apsusc.2017.01.102.
- [45] R. Sharma, K. Sehrawat, R. M. Mehra, Epitaxial growth of highly transparent and conducting Sc-doped ZnO films on c-plane sapphire by sol-gel process without buffer, Current Applied Physics 10 (1) (2010) 164–170. doi:10.1016/j.cap.2009.05.013.
- [46] J. H. Lee, B. O. Park, Transparent conducting ZnO:Al, In and Sn thin films deposited by the sol-gel method, Thin Solid Films 426 (1-2) (2003) 94–99. doi:10.1016/S0040-6090(03)00014-2.
- [47] W. Tang, D. C. Cameron, Aluminum-doped zinc oxide transparent conductors deposited by the sol-gel process, Thin Solid Films 238 (1) (1994) 83–87. doi:10.1016/0040-6090(94)90653-X.
- [48] R. D. Shannon, Revised effective ionic radii and systematic studies of interatomic distances in halides and chalcogenides, Acta Crystallographica Section A 32 (5) (1976) 751–767. doi:10.1107/S0567739476001551.

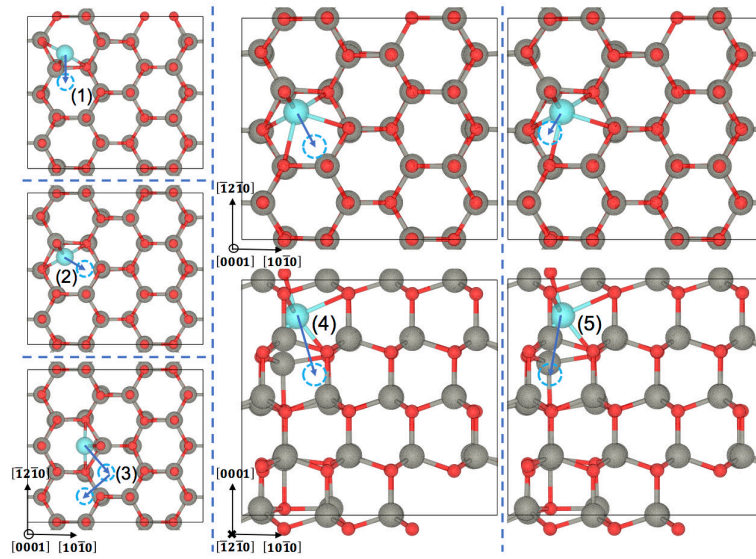


Fig. 1: Migration paths of silver interstitials along the a -, b -, and c -axes: (1) migration between interstitial sites in nearby hexagonal cages, (2) migration between interstitial sites in the same cage, and (3) migration between interstitial sites in nearby cages through a third cage. Migration paths along the c -axis: (4) migration through the centre of the hexagonal cage, and (5) migration along the edge of the hexagonal cage. The red and grey atoms represent oxygen and zinc respectively. The cyan atom is silver.

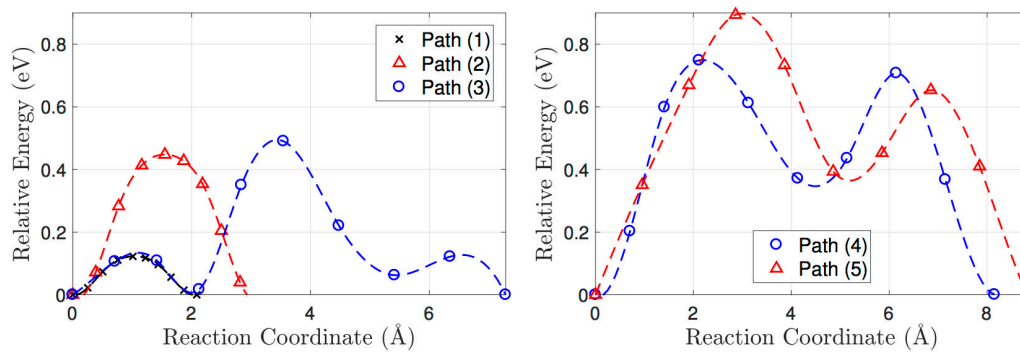


Fig. 2: Calculated MEPs for silver interstitial migration along the a -, b -, and c -axes in pure ZnO.

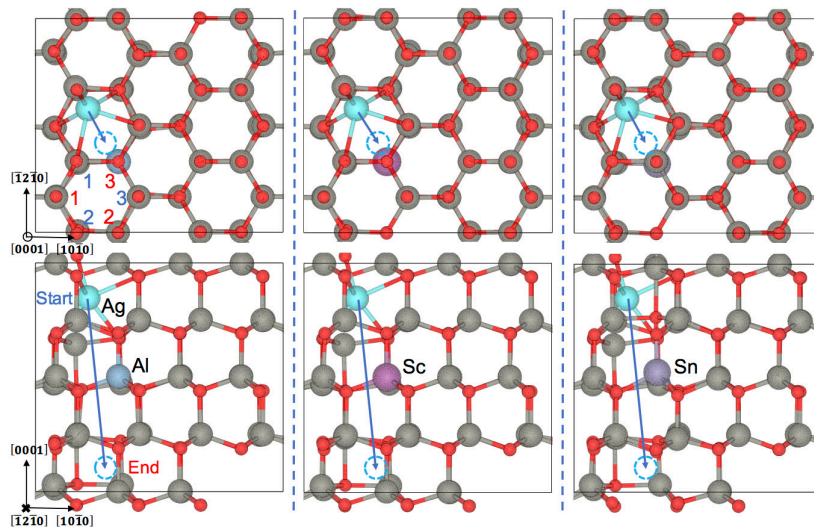


Fig. 3: Extended Ag interstitial migration paths along the c -axis in Al, Sc and Sn-doped ZnO. The three possible starting locations for the Ag atom in the hexagonal cage are shown in blue, while the three possible ending locations are shown in red. The dopant atoms are located approximately half-way along each path.

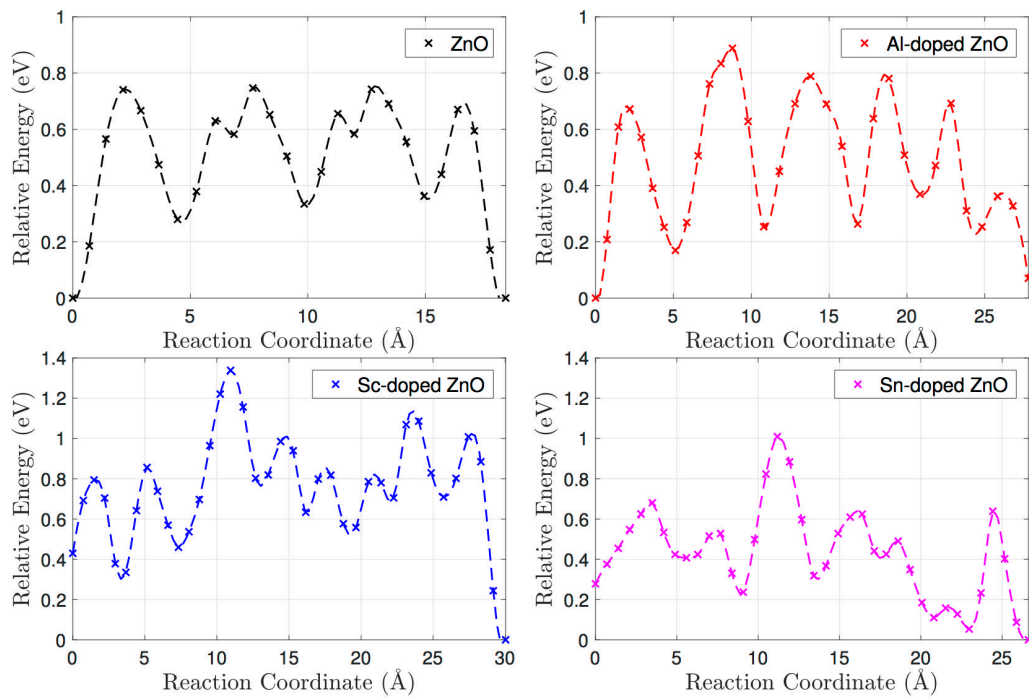


Fig. 4: Calculated MEPs for Ag diffusion in pure and doped ZnO. The migration barrier in pure ZnO (0.75 eV) agrees well with Path (4) in Table 3. Slightly larger migration barriers of 0.89 and 1.01 eV are found in Al- and Sn-doped ZnO. Sc-doped ZnO exhibits the largest barrier of 1.34 eV.

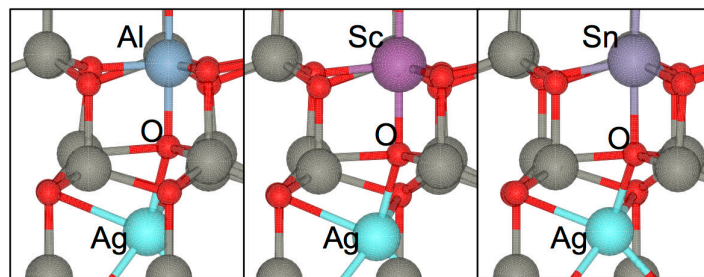


Fig. 5: Trimer configurations in doped ZnO involving the dopant, a neighbouring O atom and the migrating Ag interstitial. The trimer is bound in the case of Sc and Sn-doped ZnO whereas it is not in Al-doped ZnO.